



HAL
open science

Ultrastretchable, Highly Transparent, Self-Adhesive, and 3D-Printable Ionic Hydrogels for Multimode Tactical Sensing

Hua Wei, Zhenwu Wang, Hua Zhang, Youju Huang, Zongbao Wang, Yang Zhou, Ben Bin Xu, Sami Halila, Jing Chen

► To cite this version:

Hua Wei, Zhenwu Wang, Hua Zhang, Youju Huang, Zongbao Wang, et al.. Ultrastretchable, Highly Transparent, Self-Adhesive, and 3D-Printable Ionic Hydrogels for Multimode Tactical Sensing. *Chemistry of Materials*, 2021, 33 (17), pp.6731-6742. 10.1021/acs.chemmater.1c01246 . hal-03376651

HAL Id: hal-03376651

<https://hal.science/hal-03376651>

Submitted on 13 Oct 2021

HAL is a multi-disciplinary open access archive for the deposit and dissemination of scientific research documents, whether they are published or not. The documents may come from teaching and research institutions in France or abroad, or from public or private research centers.

L'archive ouverte pluridisciplinaire **HAL**, est destinée au dépôt et à la diffusion de documents scientifiques de niveau recherche, publiés ou non, émanant des établissements d'enseignement et de recherche français ou étrangers, des laboratoires publics ou privés.

Ultrastretchable, Highly Transparent, Self-Adhesive, and 3D-Printable Ionic Hydrogels for Multimode Tactical Sensing

Hua Wei, Zhenwu Wang, Hua Zhang, Youju Huang*, Zongbao Wang, Yang Zhou, Ben Bin Xu*, Sami Halila, and Jing Chen*

Chem. Mater. 2021, 33, 17, 6731–6742

Authors

Youju Huang – College of Material, Chemistry and Chemical Engineering, Hangzhou Normal University, Hangzhou 310036, China; National Engineering Research Centre for Advanced Polymer Processing Technology, Zhengzhou University, Zhengzhou 450002, China; orcid.org/0000-0001-5815-9784; Email: yjhuang@hznu.edu.cn

Ben Bin Xu – Department of Mechanical and Construction Engineering, Faculty of Engineering and Environment, Northumbria University, Newcastle upon Tyne NE1 8ST, U.K.; orcid.org/0000-0002-6747-2016; Email: ben.xu@northumbria.ac.uk

Jing Chen – Zhejiang International Scientific and Technological Cooperative Base of Biomedical Materials and Technology, Zhejiang Engineering Research Center for Biomedical Materials, Cixi Institute of Biomedical Engineering, Ningbo Institute of Materials Technology and Engineering, Chinese Academy of Sciences, Ningbo 315300, China; orcid.org/0000-0002-0024-4561; Email: jing.chen@nimte.ac.cn

Hua Wei – Zhejiang International Scientific and Technological Cooperative Base of Biomedical Materials and Technology, Zhejiang Engineering Research Center for Biomedical

Materials, Cixi Institute of Biomedical Engineering, Ningbo Institute of Materials Technology and Engineering, Chinese Academy of Sciences, Ningbo 315300, China; Ningbo Key Laboratory of Specialty Polymers, Faculty of Materials Science and Chemical Engineering, Ningbo University, Ningbo 315211, China

Zhenwu Wang – Karlsruhe Institute of Technology (KIT), Institute of Biological and Chemical Systems-Functional Molecular Systems (IBCS-FMS), 76344 Eggenstein Leopoldshafen, Germany

Hua Zhang – Zhejiang International Scientific and Technological Cooperative Base of Biomedical Materials and Technology, Zhejiang Engineering Research Center for Biomedical Materials, Cixi Institute of Biomedical Engineering, Ningbo Institute of Materials Technology and Engineering, Chinese Academy of Sciences, Ningbo 315300, China

Zongbao Wang – Ningbo Key Laboratory of Specialty Polymers, Faculty of Materials Science and Chemical Engineering, Ningbo University, Ningbo 315211, China; orcid.org/0000-0002-7399-4638

Yang Zhou – Zhejiang International Scientific and Technological Cooperative Base of Biomedical Materials and Technology, Zhejiang Engineering Research Center for Biomedical Materials, Cixi Institute of Biomedical Engineering, Ningbo Institute of Materials Technology and Engineering, Chinese Academy of Sciences, Ningbo 315300, China

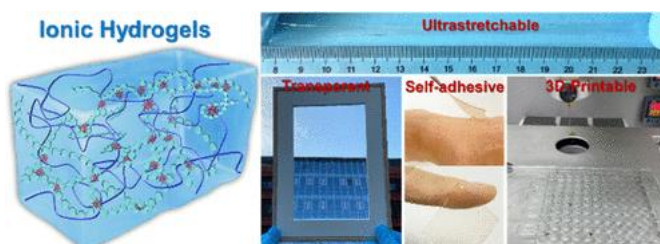
Sami Halila – Centre de Recherches sur les Macromolécules Végétales, (CERMAV, UPR-CNRS 5301), Université Grenoble Alpes, 38041 Grenoble, France; orcid.org/0000-0002-9673-1099

Abstract

Ionic gel-based electronic devices are essential in future healthcare/biomedical applications, such as advanced diagnostics, therapeutics, physiotherapy, etc.

However, considerable efforts have been devoted to integrating ultrahigh stretchability,

transparency, self-adhesion, and a low-cost manufacturing process in one material for dealing with a variety of application scenarios in the real world. Here, we describe an ionically conductive hydrogel-based electronic technology by introducing charge-rich polyzwitterions into a natural polysaccharide network. The proposed hydrogel possesses ultrahigh stretchability (975%), unique optical transmittance (96.2%), and universal conformal adhesion. The bionic hydrogel electronic devices possess superior dual force/temperature sensation with high sensitivity. Moreover, we develop dedicated sensor arrays via an additive manufacturing route and demonstrate the feasibility of monitoring physical activity or analyzing the mental state of a human body based on the multichannel signal acquisition of joint bending, pulse, vocal-cord vibration, electroencephalogram, eye movement, body temperature, etc. This all-in-one strategy based on a versatile ionic hydrogel electronic platform is anticipated to open up new tactical sensing applications in smart robotics, human-machine interfaces, and wearable monitoring systems.



1. Introduction

Natural skin, the largest organ in the human body, has a variety of characteristics including being flexible, stretchable, tough, self-healing, and the capabilities to sense external stimuli for humans to feel the world. (1-4) Skin-inspired sensors can translate environmental stimuli such as heat, (5,6) pressure, (7,8) and humidity (9,10) into detectable electronic signals, like current, resistance, or capacitance, (11-13) and thus possess great potential in smart/soft robotics, (14) personal healthcare, (15-17) and artificial intelligence. (18,19) To fully mimic skin-like tactile- and temperature-sensing capabilities and beyond, it is critical to innovate flexible conductive foundation materials with mechanical compliance and sensitive electrical signal transmission. Conventional flexible and conductive materials have been fabricated by coating a metal layer (20,21) or embedding electrical conductors (e.g., semiconductors, (22,23) MXenes, (24) silver flakes, (25) graphene, (26-28) carbon nanotubes, (29,30) and conductive polymers (31,32)) in elastomers, being sensitive to strain, pressure, or temperature changes. However, there are substantial limitations that bottleneck the future applications such as inadequate stretchability (fracture strain <100%) and unstable sensitivity at high strain due to the interfacial incompatibility between the matrix and fillers, (33-35) insufficient optical transparency, and biocompatibility in wearable applications. (36-38)

The signal transmission in biological systems relies on long-distance ion immigration rather than electron transportation. (39,40) The external stimuli can induce ion transport across cell membranes and result in dynamic polarization or depolarization of neurons to achieve various sensing functions. (41) Stretchable ionic hydrogels have been regarded as the most promising candidate to fabricate next-generation intelligent "ionic skins" via a biomimetic ion-conductive mechanism. (42) A rubber-like ionic hydrogel made by blending hydroxypropyl cellulose biopolymer fibers with poly(vinyl alcohol) (PVA) has been previously reported to simultaneously achieve high conductivity and sensitivity. (43) Yet, its opacity impedes the optical signal output, bringing extra difficulty in finding accurate attaching spots on the skin and monitoring the surface state in real-time when used for health monitoring. A transparent double-network hydrogel consisting of PVA and polyacrylamide was used to sense the external pressure. (44) Only with the aid of adhesive tapes can this pressure sensor attach onto the skin, which is not only uncomfortable for skin but also adverse to signal capture due to the weak interfacial adhesion. Although ionic skins have wide applications, challenges remain in the commercial production due to their insufficient integration of functionality required from various scenarios in the real world, like inadequate stretchability for integration, low transparency for convenient observation, (45,46) sensing inaccuracy induced by the insufficient adhesion, incompatibility for the user's skin, etc.

Charge-rich polyelectrolytes offer a high-conductivity pathway for ion transport and they can also adhere to various substrates, but their mechanical strength and elasticity remain relatively low. In this work, we synthesize an alginate network physically cross-linked by calcium ions and semi-interpenetrating copolymers consisting of zwitterionic [2-(methacryloyloxy) ethyl] dimethyl-(3-sulfopropyl) ammonium hydroxide (SBMA) and 2-hydroxyethyl methacrylate (HEMA) (Figure 1a). The reversible physical cross-link brings advantages such as energy dissipation, superelasticity, and adaptive self-adhesion due to the ion-dipole or dipole-dipole interaction created by strong dipolar zwitterionic units. (47-49) The obtained hydrogels are denoted as AHS_x, where A refers to sodium alginate, H refers to HEMA, and S refers to SBMA with a subscript x for its concentration (mol L⁻¹). They show remarkable stretchability (~975%), high optical transmittance (~96.2%), and self-adhesion to diverse substrates (Figure 1b). The hydrogels also present high ionic conductivity (0.39 S m⁻¹) and sensitivity (up to 3.26 and 7.34 of the gauge factor for the tensile and compressive strain responses, respectively, and up to 2.39%/°C of the temperature coefficient of resistance for the temperature response). By utilizing the 3D printing technique, we create a prototype of sensor arrays with designable structures to detect force or temperature signals in 1-D and 2-D. This work demonstrates a multimodal sensing strategy using an ionically conductive hydrogel to comprehensively assess bioactivities of the human body in real-time, which holds promises in the applications of wearable healthcare devices.

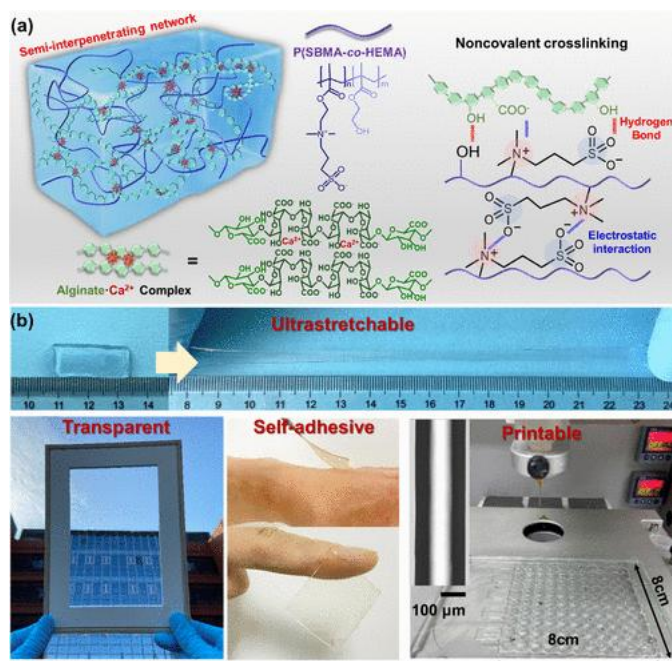


Figure 1. (a) Schematic illustration of the alginate/P(SBMA-co-HEMA) hydrogel (AHS) with a semi-interpenetrating network cross-linked by reversible noncovalent interactions. (b) Comprehensive fulfillment of its ultrastretchability, transparency, adhesion, and printability for dual force/temperature sensation.

2. Results and Discussion

2.1. Basic Properties of the AHS Hydrogels

Naturally derived alginate contains consecutive or alternating (1,4)-linked β -d-mannuronate (M) blocks and α -l-guluronate (G) blocks, where the adjacent G blocks can chelate divalent or multivalent metal ions to form ion-cross-linked networks. (50,51) To avoid the formation of an inhomogeneous network due to the rapid ion releasing process, Ca^{2+} was controllably released by an ethylenediaminetetraacetic acid calcium disodium salt (EDTANa_2Ca)/d-(+)-gluconic acid δ -lactone (GDL) system to create a uniform rigid skeleton (52) (Figure S1). The sulfonic acid anions of SBMA can interact with ammonium cations via electrostatic force to generate extra cross-linking bonds. The abundant hydroxyl and carboxylic acid groups of alginate can initiate the hydrogen bonding and electrostatic interaction in a macromolecular system, identified by the peak shift of OH and S=O bands in the FTIR spectra (Figure S2), yielding a dual physical cross-linking network (53) (Figure 1a). The alginate hydrogel is reinforced by introducing interpenetrative polymer chains with a tensile strength of 294.9 ± 13.2 kPa and a tensile strain of $906.7 \pm 37.9\%$ of $\text{AHS}_{1.5}$ (Figures 2a and S3a) and a maximum compression strength of 15.14 ± 1.2 MPa and compressive strain of 98% for $\text{AHS}_{1.5}$ (Figure S3b,c). On the contrary, the sole calcium alginate hydrogel (Alg) presents a fracture tensile stress of 71.7 ± 6.1 kPa at a strain of $121.8 \pm 22.2\%$ and a fracture compression strength of 0.07 ± 0.01 MPa at a strain of $52.9 \pm 1.6\%$. Their elastic moduli and toughness elevate as the SBMA contents are increased from 0.5 to 1.5 mol L^{-1} , and subsequently slightly drop below the maximum values (Figure S3d).

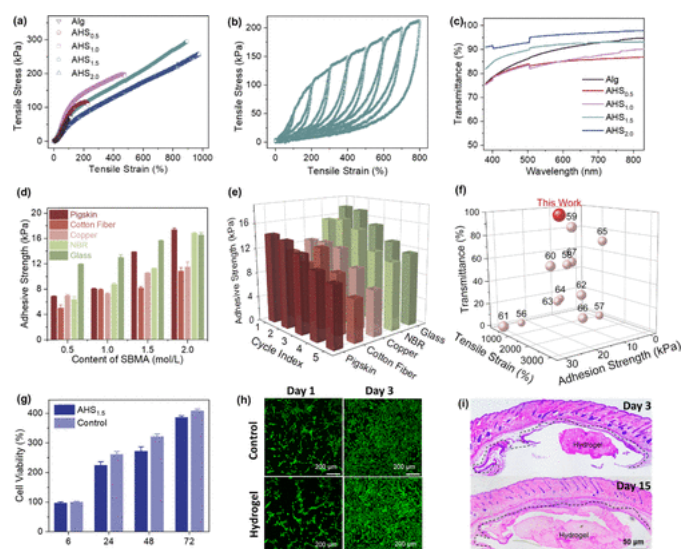


Figure 2. (a) Representative tensile stress–strain curves of the AHS_x hydrogels with different SBMA contents in the precursor solutions from 0.5 to 2.0 mol L⁻¹. (b) Cyclic tensile loading–unloading curves of the AHS_{1.5} hydrogel under gradually increased strains (100, 200, 300, 400, 500, 600, 700, and 800%). The relaxing time after each cycle is 1 h. (c) Transmittance of the AHS_x hydrogels in the visible range. (d) Adhesion strength of the AHS_x hydrogels with different SBMA contents to diverse substrates and (e) repeated adhesion of the AHS_{1.5} hydrogel adhered to different substrates for five cycles. (f) Comparison of tensile strain, transmittance, and adhesion strength of reported conductive hydrogels. (56–67) (g) Evaluation of cytotoxicity and cell proliferation using CCK-8 assay on 3T3 cells cocultured with extracts of the AHS_{1.5} hydrogel and control (cell culture medium) for 6, 24, 48, and 72 h. (h) Laser scanning confocal microscopy images of live/dead staining on 3T3 cells cocultured with extracts of the AHS_{1.5} hydrogel and control for 24 and 72 h. (i) HE staining after 3 and 15 days of subcutaneous implantation.

Such mechanical reinforcement induced by the interpenetrative P(SBMA-co-HEMA) copolymer chains also brings an advantage to dissipate energy upon external loading. When the AHS_{1.5} hydrogel was immersed in a saturated NaCl solution for 1 h, the tensile strength of the hydrogel significantly decreased (Figure S4). We speculate that both Cl⁻ and Na⁺ ions permeated into the hydrogel network and interacted with the cationic quaternary ammonium and anionic sulfonate groups of SBMA units to cause electrostatic shielding. The generated electrostatic interaction significantly disassociates polymer chains, enabling them to lose partial capability to dissipate energy upon external loading. Since SBMA simultaneously has H bonding acceptor (S=O) (54,55) and positively charged quaternary ammonium, the SBMA unit within the network is conducive to enhance the capability of energy dissipation through supramolecular interaction with functional groups (OH and COOH) of alginates. Yet, the interpenetrative chains also tend to assemble with each other via interchain electrostatic force to form a microscopic phase when the SBMA content surpasses a certain value, yielding an inhomogeneous network structure with slightly reduced mechanical performances.

We examine the mechanical endurance and structural stability by performing cyclic loading–unloading tensile (Figure 2b) or compression (Figure S3e) tests for the AHS_{1.5} hydrogel, which show pronounced hysteresis loops. The interplay between Ca²⁺ and alginate not only constructs a rigid network to dissipate energy but also restrains the slippage of P(SBMA-co-HEMA) chains to maintain the network. The hysteresis loops shown in cyclic loading–unloading tensile tests at different strains suggest a disintegration of the network due to the possible disassociation of alginate/Ca²⁺ complexation (Figure 2b). To recover such ionic complexation, the hydrogel sample was relaxed for 1 h to perform the following cyclic test. It is found that the stress values in loading processes are comparable with those at the same strains in the tensile test, indicating partial network recovery due to the reversible alginate/Ca²⁺ complexing interaction. During 50 cycles of compression, the hysteresis loops demonstrate a remarkable overlap after the first cycle (Figure

[S3e](#)), exhibiting robust strength and toughness ([Figure S3f](#)). Similar trends are also found in the cyclic tensile ([Figure S3g](#)). It seems that the alginate/ Ca^{2+} complexation undergoes a saturation in the first loading with some decoupling and recoupling to generate a reversible noncovalent cross-linking network with good recovery since the second cycle.

While optical transparency endows the electronic devices with unobtrusive visual appearance, it also enables precision in targeting the specific areas for the real-time monitoring of motions or signals. As a fully water-soluble polysaccharide, the Alg hydrogel shows a high transmittance of 80–90% at a wavelength range of 400–800 nm ([Figure 2c](#)). However, the transmittance of AHS_{0.5} and ASH_{1.0} gels decline to 75–85% because the interpenetrative P(SBMA-co-HEMA) chains in the AHS_x hydrogels can randomly aggregate into a microphase via the hydrophobic interaction of HEMA moieties with a relatively low SBMA content ($x = 0.5$ and 1.0). Interestingly, the transmittance of the AHS_{1.5} and AHS_{2.0} hydrogels ramp up to above 90% ([Figure 2c](#)), when the SBMA content further increases. An explicit decrease in the crystallization of alginate is observed in the XRD spectrum of the AHS hydrogel ([Figure S5](#)), which may contribute to the high optical transparency.

Mechanical compliance and durability are critical for the signal transmission of ionic skins, where the conformal adhesion could adaptively overcome the interfacial gaps and enhance the sensitivity of signal capture. ([68](#)) The hydrogel can firmly adhere to diverse surfaces (*e.g.*, human skin, nitrile butadiene rubber, glass, *etc.*, [Figure S6](#)). We demonstrate a conformal adhesion of the AHS_{1.5} hydrogel on the human skin ([Video S1](#)). The AHS_{1.5} hydrogel tightly stuck to the skin even under a drastic shaking and could be easily peeled off without any residue. We also find that the adhesion strength of the AHS_{1.5} hydrogel upon porcine skin (a human skin simulant) was 13.84 kPa, whose adhesion is stronger than the fibrin glue (~12 kPa) that is used in clinics ([69](#)) ([Figure 2d](#)). The adhesion property is attributed to the high polarity of zwitterionic polymers within the hydrogels. Both charged groups (cationic quaternary ammonium and anionic sulfonate) and polar groups ($\text{S}=\text{O}$) tend to interact with other charged or polar groups on the surface of most substrates through ion–dipole and/or dipole–dipole interactions, resulting in a strong interfacial bonding. ([70](#)) Such intrinsic adhesive features allow the AHS hydrogel to be used in human–machine interaction, soft robotics, *etc.*, in a patch-in fashion. Furthermore, cyclic shear tests of the AHS_{1.5} hydrogel upon various substrates are performed ([Figure 2e](#)). The adhesion strength shows a gradual decrease during the cyclic adhesion–peeling processes, probably due to the contamination and/or the accumulated fracture on the hydrogel after each cycle. [Figure 2f](#) provides a summary of the electron- or ion-conductive flexible materials reported to date from the perspectives of stretchability, transparency, and adhesion, where our AHS hydrogels stand out with an unprecedented comprehensive superiority over other reported materials.

We also evaluate the biocompatibility of the AHS hydrogel by coculturing 3T3 cells with cylindrical hydrogel sheets at a density of 1×10^5 cells per mL. Compared with the control group, the AHS hydrogel showed no significant cytotoxicity to 3T3 cells and the cells displayed obvious proliferation after 6, 24, 48, and 72 h ([Figure 2g](#)). Moreover, no statistical difference was observed in the cell viability between the hydrogel group and the control one. After assessing the morphology of 3T3 cells after 24 h of coculture by live/dead staining assay, cells present a healthy spindle morphology with a consistent cell density on the surface of the AHS gel ([Figure 2h](#)), indicating good biosafety. We find that the CD68⁺ macrophage invasion (green fluorescence) at the hydrogel–tissue interface occurred at day 3 but almost disappeared at day 15, indicating that there is a mild and early inflammatory response to the hydrogel ([Figures 2i](#) and [S7](#)), which confirms good biocompatibility for our AHS hydrogels.

2.2. Deformation and Temperature Sensitivities of the AHS Hydrogels

The interpenetrative polyzwitterionic chains within a hydrogel network provide an ionic transportation pathway to achieve ionic conductivity. The conductivity is increased from 0.00067 to 0.39 S m^{-1} as the SBMA content increases from 0 to 2.0 mol L^{-1} , which is comparable to the conductivity of lithium copolymer polyzwitterion materials ([71](#)) ([Figure S8a](#)). We measured the deformation-dependent resistance change by tensile testing ([Figure 3a](#)), where a monotonic increase in the resistance was found by changing the tensile strain from 0 to 890% for the AHS_{1.5} hydrogel,

which is in line with a fitting quadratic equation. Such nonlinear dependence is due to the nonlinear density evolution of transport carriers of a conductive network upon strain. We speculate that the hydrogel network deforms elastically in the region of small strain. With gradually increasing the strain, the breakage of noncovalent interactions (electrostatic force, H bonding, and ion complexation) as well as the disentanglement or slippage of interpenetrative polymer chains also contributes to the network deformation. The corresponding strain sensitivity, known as the gauge factor (GF), shows a linear increase from 0.88 to 3.26 with the strain ranging from 0 to 890%. In addition, both the resistance change ratio and GF were increased with the SBMA content at a given strain due to the densified transport carriers of the hydrogel network (Figure S9). By measuring the conductivities of the AHS_{1.5} hydrogel at various strains (Figure S8b), we find that the conductivity is sensitive to the tensile strain with a nearly negative linear correlation.

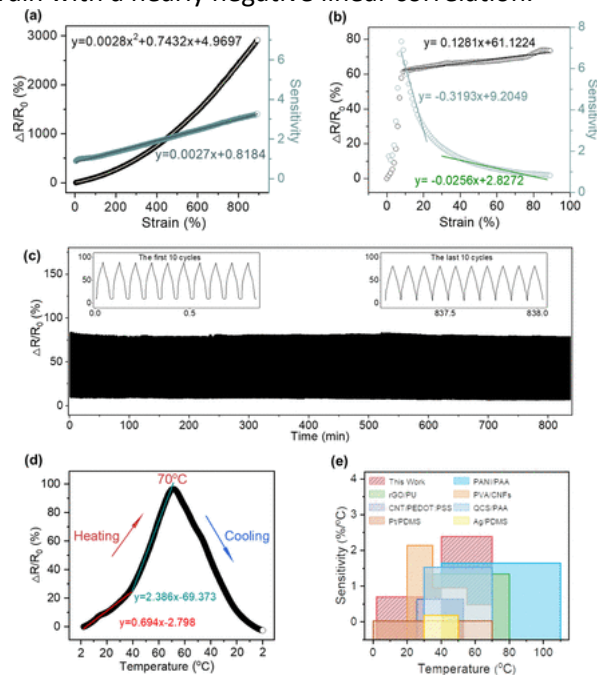


Figure 3. Dependence of the resistance change ratio and sensitivity of the AHS_{1.5} hydrogel on (a) tensile strain and (b) compressive strain. (c) Cyclic stability test of the AHS_{1.5} hydrogel under 50% compressive strain for 10 000 cycles (the duration of each cycle is 5 s). (d) Dependence of the resistance change ratio and sensitivity (TCR) of the AHS_{1.5} hydrogel on temperature (R_0 refers to the resistance of the hydrogel at 2 °C). (e) Comparison of thermosensation capabilities of documentary flexible conductive materials: Pt/poly(dimethylsiloxane) (PDMS), (5) polyaniline (PANI)/poly(acrylic acid) (PAA), (61) quaternized chitosan (QCS)/PAA, (72) poly(vinyl alcohol) (PVA)/cellulose nanofibrils (CNFs), (73) carbon nanotube (CNT)/poly(3,4-ethylenedioxythiophene)-poly(styrenesulfonate) (PEDOT:PSS), (74) reduced graphene oxide (rGO)/polyurethane (PU), (75) and Ag/PDMS. (76) Figure 3b shows a dramatic increase in the resistance change ratio with a high sensitivity of 7.34 to a minor compression up to 8.3%. The resistance change ratio slightly decreases and then becomes stable when the compressive strain further increases. We speculate that the interpenetrative copolymer chains become more and more contacted within the calcium alginate skeleton, resulting in increasing dense transportation. The conductivity of the hydrogel thus increases to achieve a sharp increase in the resistance change ratio at low strain. Although the network of the hydrogel is continuously deformed with increasing the compressive strain, the configuration and rearrangement of interpenetrative copolymer chains suffer from limited deformation space. Such high sensitivity at low compressive strain is highly required for ionic skins because the hydrogel can detect a weak pressure signal when it contacts an object. The long-term electrical stability of the AHS_{1.5} hydrogel was evaluated under cyclic compressive tests at a strain of 50% for more than 10 000 times. The resistance change ratio remained constant under repeated loadings, demonstrating its remarkable electrical stability and durability when used for practical applications (Figure 3c).

The human skin can detect a subtle change in temperature with a resolution down to 0.02 °C; (77) another perspective study is thus to investigate the temperature sensitivity of our AHS hydrogels. Figure 3d shows the resistance change ratio as a function of temperature from 2 to 70 °C during the heating and cooling processes at a rate of 1 °C min⁻¹. The resistance change ratio of the hydrogel dramatically increases with increasing temperature and decreases during the cooling process to show an approximate symmetry with those in the heating process. Note that the nonlinear evolution of the resistance change ratio in the whole temperature range is proper due to the nonlinear accelerating movement of ions and polymer chains with increasing temperature. The value of the temperature coefficient of resistance (TCR) is defined as $(\Delta R/R_0)/\Delta T$ to represent the sensitivity of thermal response. For example, the curve was linearly fitted with two slopes of 0.69%/°C (2–40 °C) and 2.39%/°C (40–70 °C) to calculate TCR, exhibiting higher sensitivity than the materials previously reported (Figure 3e). The temperature-dependent sensitivity is characterized by summarizing the conductivities of the hydrogel at different temperatures (Figure S8c), where the conductivity is found to slightly increase with an increase in temperature up to ~30 °C, followed by a sharp increase until 70 °C. This could be attributed to the accelerating movement of ions and polymer chains at a higher temperature, making ion transport easier. (78) The dynamic network can be reinforced upon heating due to the LCST nature of interpenetrative P(SBMA-co-HEMA) copolymer chains at a critical temperature ~30 °C. (79) This can be confirmed by the evolution of the storage modulus of the hydrogel during the heating and cooling processes (Figure S8d), where G' gradually increases with temperature at a critical point of ~30 °C and then decreases upon cooling to recover the initial value. In addition, we are aware of the dehydration issue that is a common challenge for hydrogel-based flexible sensors, especially when they are used for thermosensation at high temperature. Although organohydrogels (80) or ionogels (81,82) have a comparative advantage in terms of antidehydration, the dehydration issue could be alleviated to some extent because our hydrogels consisting of hydrophilic polysaccharide and a highly polar zwitterionic polymer exhibit strong hygroscopicity. In addition, our hydrogels mainly focus on the application in the field of multichannel monitoring of physiological signals (vide infra) including body temperature, that is, in fact, follows in a narrow range (30–40 °C), with a relatively low priority of concern to antidehydration.

2.3. Demonstration of Multimode Tactical Sensing

A thin layer of the AHS hydrogel is attached to the finger to demonstrate the detection of the bending gesture at different angles (Figure 4a). A logic response can be realized with the finger bending to 30, 60, and 90°, generating stable and reversible $\Delta R/R_0$ data of 14, 20, and 28%, respectively. This demonstration has been extended to record the finger bending at different frequencies synchronously (Figure S10a) and track high-amplitude motions of arms and legs in real-time (Figure S10b,c). The hydrogel device is connected with an electrical circuit to detect the typical vibration peaks of the human pulse (Figure 4b), and a real-time signal sequence can be exported to a commercial cardiac monitor display. We also utilize the bionic gel to monitor the subtle muscle movement during verbal communication (Figure 4c) by mounting the gel device on the neck of the speaker. A signature of voice can be recorded digitally in response to the different words that the speaker pronounced, suggesting a great potential in the applications of speech recognition and artificial intelligence (AI).

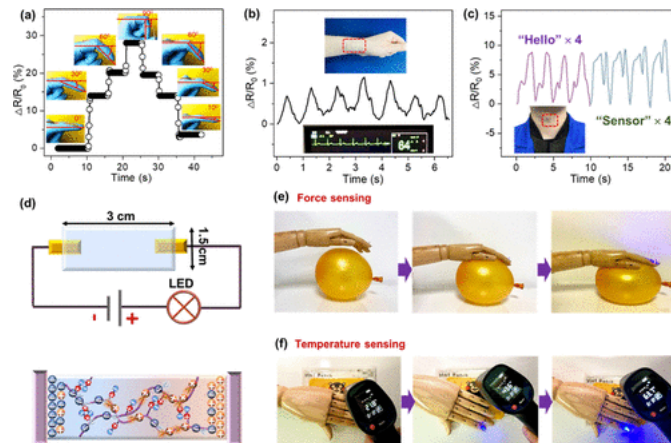


Figure 4. Time-dependent resistance change-based real-time monitoring for (a) finger bending at different angles, (b) pulse beat, and (c) vocal-cord vibration. (d) Schematic illustration of the hydrogel-based sensor with (e) force and (f) temperature dual-sensory capabilities for robotics when it approaches a (e) balloon and a (f) self-heating hot patch, respectively, based on the ionic conducting mechanism.

A smart system was built to further simulate the human perception toward critical stress and temperature using a hydrogel thin layer, DC power supplier, and an LED as an indicator (Figure 4d). Once the artificial hand contacted and gripped a balloon, the LED was instantly lightened because the resistance of the hydrogel sensor decreased upon compressive pressure and the loop current increased accordingly. The LED became brighter when the artificial hand imposed a larger force to make the balloon severely deformed (Figure 4e). A temperature alerting function was triggered as the LED turned on when the artificial hand approached a self-heating hot patch (Figure 4f). With these dual-sensing capabilities, the AHS hydrogels offer promising potentials to be used in the human–machine interface to help disabled people to restore their consciousness toward force and temperature. (83)

In addition to monitoring and restoring the physiological function, there has been a growing requirement for dealing with mental health problems, which are common worldwide including frequently happening depressive and anxiety disorders. Since most mental health disorders are chronic and easy-to-relapse, it is essential to achieve a long-term follow up and assessment for symptom reduction and recovery. Ecological momentary assessment (EMA), (84) an alternative to traditional retrospective reports, allows to *in situ* sample thoughts, feelings, and behaviors as close in time to the experience of patients as possible. It has been shown that human’s mental state can be manifested through multiple physiological signals such as electroencephalogram (EEG), eye movement (EM), body temperature, *etc.* (85) Therefore, we propose a proof-of-concept of multimode tactical sensing at the same time to produce more informative results compared to single sensing modality (Figure 5a). Benefited from the self-adhesive and conductive natures of AHS hydrogels, a size-matched hydrogel column was finely embedded into the EEG probe (Figure 5b), with a tight contact with the skin and comparable conductivity to commercially used conductive cream, which is made of carboxymethylcellulose. As a control, the second EEG probe was filled by commercial cream. The other two hydrogel patches were fixed on forehead and canthi, respectively. In this way, four signal channels can synchronously work to record the evolution of EEG, EG, and temperature thanks to the integrated natures of AHS hydrogels, including ionic conductivity, strain sensing, and temperature sensing (Figure 5c). Note that an obvious electromyographic (EMG) signal can also be recorded accompanied with each blinking movement. Using this multimodal sensing setting as a wearable device in future, it is helpful to extract meaningful information from multidimensional sensing data to build the inherent relationship between external physical signals and the mental state of humans, which is potentially valuable in clinical diagnosis and therapeutic applications in near future. (86)

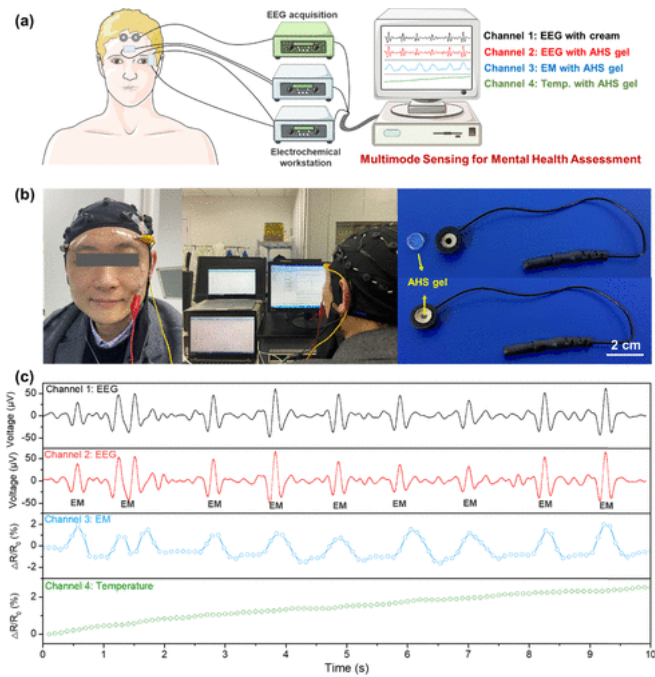


Figure 5. (a) Schematic illustration of multimode sensing for mental health assessment. (b) Four-channel arrangement and the EEG probe using an as-prepared AHS hydrogel. (c) Time-dependent voltage and resistance change-based real-time monitoring for EEG, EM, and forehead temperature (the forehead of volunteer was precooled at 0 s).

A feasible scale-up manufacturing technique plays a crucial role in the lab-to-fab translation of smart skin-like sensors. (87) Here, we introduce a 3D printing approach to fabricate AHS hydrogel-based sensor array. The printability of the hydrogel originates from the tunable viscoelasticity of the precursor solution before thermally initiated polymerization (Figure S11 and Video S2). The time-lapse rheological measurement suggests a stable modulus value of an ion-cross-linked polysaccharide skeleton containing monomers ($G' = \sim 200$ Pa, $G'' = \sim 35$ Pa) over 600 s, leading to an efficient and steady extrusion for printing (Figure S11a). A characteristic gel-sol transition was also found at an oscillation strain of 430% (Figure S11b). A switchable fluctuation between high (1000%) and low (1%) strains (Figure S11c) suggested a reversible gel-to-sol-to-gel process, with a quick self-healing capability. The superior gelation, unique shear-induced gel-sol transition, and rapid self-healing capability fulfill a direct extrusion-based 3D printability to the precursor. A 9×9 pixel array (8×8 cm²) (Figure 6a) was rapidly fabricated after 5 min, with an excellent conformability to the skin (Figure 6b). Benefited from such array architecture, outstanding resistance change ratios from these pixels are recorded and reproduced in a computer, in which no signal cross-talk occurred. The as-fabricated sensor array can accurately map the pressure or temperature distribution via the resistance-dependent color contrast, which is in consistency with the shape of force donor (e.g., two fingers) (Figure 6c) or a heat source (e.g., hair dryer) (Figure 6d). Moreover, a more complex integrated device could also be manufactured by virtue of 3D printability of our hydrogels. In this way, strain and temperature sensing could independently run without interfering with each other in real-world applications.

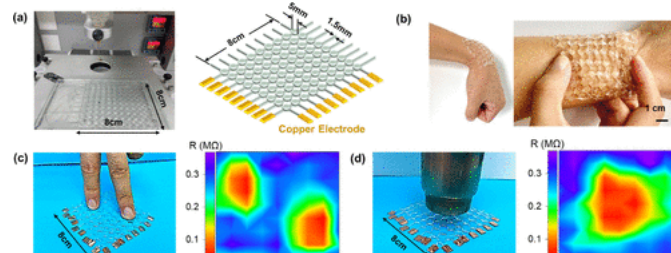


Figure 6. (a) Three-dimensional (3D)-printed AHS_{1.5} hydrogel sensor array with 9×9 pixel (8×8 cm²). (b) Pictures of the sensor array on the wrist and under wrinkling to show its conformality with the

skin. Pictures of (c) two-finger pressing on the sensor array and (d) heating above the sensor array with a real-time 2-D mapping of resistance change. The corresponding mapping profiles of pixel signals are shown on the right.

3. Conclusions

We propose an ionically conductive hydrogel with the satisfactory fulfillment of biocompatible, ultrastretchable, transparent, self-adhesive, and 3D printable natures for multimode tactical sensing. The physical cross-linking network through reversible hydrogen bonding and electrostatic interactions enables an ultrastretchability as high as 975%. The hydrogel also presented a unique optical transmittance (96.2%) and universal adhesion with different substrates. In addition, a sensor array can be fabricated by the facile and large-scalable additive manufacturing method, opening a new window for the future scale-up manufacturing. The hydrogel electronic devices are capable of accurate deformation and temperature sensitivities. We demonstrate the application of ionic gel electronics for multimode tactical sensing. These advantages in functionality and manufacturing shed light on various promising applications such as motion capture, physiological and psychological health assessment, and human-machine interface.

4. Experimental Section

4.1. Chemicals

[2-(Methacryloyloxy) ethyl] dimethyl-(3-sulfopropyl) ammonium hydroxide (SBMA, 97%), 2-hydroxyethyl methacrylate (HEMA, 96%), d-(+)-gluconic acid δ -lactone (GDL), ethylenediaminetetraacetic acid calcium disodium salt hydrate (EDTANa₂Ca), sodium alginate, and 2'-azobis(2-methyl-propionamide) dihydrochloride (V-50, 99%) were purchased from Aladdin (China) and used as received without purification. Deionized water with a resistivity of 18.2 M Ω cm⁻¹ was prepared using an ELGA LabWater system (France).

4.2. Preparation of Ion-Conductive Hydrogels

The ion-conductive hydrogels were prepared by a one-pot [\(88\)](#) and two-step procedure. In a typical synthesis, an aqueous solution of sodium alginate (3 wt %) was first prepared by vigorously stirring at 60 °C. After the addition of EDTANa₂Ca, HEMA, SBMA, and initiator V-50 into the solution, the mixture was stirred for 30 min to form a thick solution. The formulations for the preparation are shown in [Table 1](#). All solutions were degassed by centrifugation at 8000 rad min⁻¹. Subsequently, GDL was added to the solution to trigger the release of Ca²⁺ ions for cross-linking alginate. After degassing by centrifugation at 5000 rad min⁻¹, the mixed solution was then transferred into a mold composed of a silicone rubber spacer (thickness = 1.5 mm) between two glass plates. The mold accommodating the precursor solution was kept at room temperature for 3 h to form the alginate network cross-linked by Ca²⁺ ions, and then placed in a water bath at 40 °C for 24 h to in situ initiate the copolymerization of SBMA and HEMA.

Table 1. Formulations of the Precursor Solutions for the Preparation of AHS_x Hydrogels

sample	alginate (wt %)	SBMA (mol L ⁻¹)	HEMA (mol L ⁻¹)	EDTANa ₂ Ca (mmol L ⁻¹)	GDL (mmol L ⁻¹)	V-50 (mmol L ⁻¹)
Alg	3	0	0	150	225	0
AHS ₀	3	0	1	150	225	5.0
AHS _{0.5}	3	0.5	1	150	225	7.5
AHS _{1.0}	3	1.0	1	150	225	10.0
AHS _{1.5}	3	1.5	1	150	225	12.5
AHS _{2.0}	3	2.0	1	150	225	15.0

4.3. Characterization

The chemical structures of freeze-dried hydrogels were analyzed at room temperature using a Fourier transform infrared (FTIR) spectrometer (Micro-FTIR, Agilent Cary 660) in a transition mode. All of the spectra were obtained with 32 scans and a resolution of 4 cm^{-1} in a range of $4000\text{--}400\text{ cm}^{-1}$. The transmittance spectra of the hydrogels (thickness = 1.5 mm) were characterized on a UV-vis spectrophotometer (Lambda 950 UV-vis-NIR spectrophotometer) with a wavelength ranging from 800 to 400 nm, and the transmittance of air was measured as the baseline. The crystalline nature of the hydrogels was characterized by wide-angle X-ray powder diffraction (XRD) on a D8 Advance Davinci X-ray diffractometer (Bruker, Germany) under a wavelength of 1.5406 \AA ($K\alpha$ emission). The scanning speed was 10° min^{-1} and the data were transformed to one-dimensional patterns of intensity versus scattering angle. Rheological tests were carried out on a TA Instrument DHR-2 Rheometer at $25\text{ }^\circ\text{C}$, using a 20 mm measuring plate.

4.4. Mechanical Tests of the Hydrogels

The mechanical performances of hydrogels were investigated using a Universal Testing Machine (Instron 5567). Tensile tests were performed on three parallel dumbbell-shaped specimens ($2\text{ mm} \times 10\text{ mm} \times 1.5\text{ mm}$) at a cross-head speed of 100 mm min^{-1} . Cylindrical samples (1.5 mm in height and 13 mm in diameter) were used for compression tests at a speed of $10\% \text{ min}^{-1}$. The fracture toughness of each sample was calculated by integrating the area under the stress-strain curve. Successive tensile cycle tests (up to 100% of strain) and compressive cycle tests (up to 80% of strain) were further performed to investigate the tough performance of hydrogels.

4.5. Adhesion Measurements of the Hydrogels

The adhesion performances of the hydrogels on various surfaces were determined by lap shear tests using a Universal Testing Machine (Instron 5567). In a typical measurement, a hydrogel was sandwiched between two pieces of glass with an overlapping area of $2.5\text{ cm} \times 2.0\text{ cm}$. To measure the adhesion of the hydrogel with different surfaces, a cotton fabric, copper sheet, rubber, or porcine skin was fixed on the glass surface in advance. To achieve sufficient contact, the sandwich-like specimen was pressed by a weight (100 g) for 10 min before the test ([Figure S12a](#)). All tests were performed at a shear rate of 100 mm min^{-1} at room temperature. The test for each sample was repeated at least three times and the results were reported as mean standard deviation. The adhesion strength was determined by the maximum force divided by the known overlapping area of the adhesive joint ([Figure S12b](#)).

4.6. Electrical Measurements of the Hydrogels

The conductivity of hydrogels was measured using a digital four-probe tester (Jingge ST2258C, China). The resistance changes of the hydrogels were obtained using an electrochemical workstation (CHI600E, China). The gauge factor (GF) is defined as $GF = [|R - R_0|/R_0]/\epsilon = (\Delta R/R_0)/\epsilon$, where R_0 and R are the resistances of the original and loaded hydrogels, respectively, and ϵ is the strain of the hydrogel. Real-time change of strain was realized by a Universal Testing Machine, and real-time change of temperature from 2 to $70\text{ }^\circ\text{C}$ was controlled by a TA Instruments DHR-2 Rheometer. All noninvasive experiments for monitoring human physiological signals were performed with the consent of the volunteers.

4.7. Three-Dimensional (3D) Printing Fabrication of Sensor Arrays

A 3D Discovery bioprinter (RegenHU, 3D Discovery, Switzerland) was used to print the target construct of sensor arrays. The precursor solution before polymerization was transferred into the extruder and printed into target array construct using the same print settings: a 20 G nozzle, line width = $500\text{ }\mu\text{m}$, layer height = $350\text{ }\mu\text{m}$, print head speed = 12 mm s^{-1} , dosing pressure = 0.04 MPa, radius of each circular shape = 4 mm, interval between circles = 4 mm, and thickness of array = 0.5 mm. The printed matrices were further put into a water bath at $40\text{ }^\circ\text{C}$ for polymerization.

4.8. Biocompatibility Evaluation

For cytocompatibility studies, the mouse fibroblasts cells (NIH/3T3) were seeded at a density of 1×10^5 cells per mL on a 20 mm confocal dish (Corning, American). Subsequently, the sterilized AHS_{1.5} hydrogels were immersed in growth media (low-glucose Dulbecco's modified Eagle medium (DMEM, Gibco) supplemented with 10% fetal bovine serum (FBS, Gibco) and 1% penicillin/streptomycin (Gibco)). After 6, 24, 48, and 72 h coculture in a humidified incubator at $37\text{ }^\circ\text{C}$

with 5% CO₂, the cell viability was evaluated using a CCK-8 kit according to the protocol (Beyotime, China). In addition, the cell viability and morphology were determined by live/dead assay according to the manufacturer's protocol (Biovision). Images were visualized using a laser scanning confocal microscope (LSCM, Leica TCS-SP8, Germany). The histocompatibility of hydrogels *in vivo* was carried out via subcutaneous implantation in 8-week-old ICR mice (25–30 g) housed in the Animal Service Centre of Ningbo University. All animal experiments were performed in compliance with the guidelines for the Care and Use of Research Animals established by the Institutional Animal Ethical Committee (IAEC) of Ningbo University. All surgical procedures were approved by the Institutional Animal Ethical Committee (IAEC) of Ningbo University. Tissue samples were harvested from euthanized mice at 3 and 15 days, and immediately fixed in 10% neutral buffered formalin overnight at 4 °C and embedded in paraffin. Subsequently, the embedded samples were sectioned perpendicularly to the skin surface in 6 μm consecutive sections. The sections were stained with immunohistochemical staining with CD68 antibodies (1:200, Abcam). Fluorescence microscopy images were obtained using an LSCM (Leica TCS-SP8, Germany).

Supporting Information

The Supporting Information is available free of charge at <https://pubs-acsc.org/gaenomad-1.grenet.fr/doi/10.1021/acs.chemmater.1c01246>.

- The controlled release mechanism of Ca²⁺ for cross-linking alginate, and additional FTIR spectra, mechanical testing, XRD, rheological testing, adhesion strength, conductivity, resistance, and immunohistochemical results ([PDF](#))
- A conformal adhesion of the AHS_{1.5} hydrogel on the human skin ([MOV](#))
- A 3D printing approach to fabricate AHS hydrogel-based sensor array ([MOV](#))

REFERENCES

- (1) Roosterman, D.; Goerge, T.; Schneider, S. W.; Bunnett, N. W.; Steinhoff, M. Neuronal Control of Skin Function: The Skin as a Neuroimmunoendocrine Organ. *Physiol. Rev.* 2006, 86, 1309–1379.
- (2) Rees, J. Understanding Barrier Function of the Skin. *Lancet* 1999, 354, 1491–1492.
- (3) Lee, Y.; Park, J.; Choe, A.; Cho, S.; Kim, J.; Ko, H. Mimicking Human and Biological Skins for Multifunctional Skin Electronics. *Adv. Funct. Mater.* 2020, 30, No. 1904523.
- (4) Di Meglio, P.; Perera, G. K.; Nestle, F. O. The Multitasking Organ: Recent Insights into Skin Immune Function. *Immunity* 2011, 35, 857–869.
- (5) Hua, Q.; Sun, J.; Liu, H.; Bao, R.; Yu, R.; Zhai, J.; Pan, C.; Wang, Z. L. Skin-Inspired Highly Stretchable and Conformable Matrix Networks for Multifunctional Sensing. *Nat. Commun.* 2018, 9, No. 244.
- (6) Park, J.; Kim, M.; Lee, Y.; Lee, H. S.; Ko, H. NaturematerialsFingertip Skin-Inspired Microstructured Ferroelectric Skins Discriminate Static: Dynamic Pressure and Temperature Stimuli. *Sci. Adv.* 2015, No. 1500661.
- (7) Tee, B. C.; Wang, C.; Allen, R.; Bao, Z. An Electrically and Mechanically Self-healing Composite with Pressure- and FlexionSensitive Properties for Electronic Skin Applications. *Nat. Nanotechnol.* 2012, 7, 825–832.
- (8) Huang, Y.; Fan, X.; Chen, S. C.; Zhao, N. Emerging Technologies of Flexible Pressure Sensors: Materials, Modeling, Devices, and Manufacturing. *Adv. Funct. Mater.* 2019, 29, No. 1808509.
- (9) Cheng, Y.; Wang, J.; Qiu, Z.; Zheng, X.; Leung, N. L. C.; Lam, J. W. Y.; Tang, B. Z. Multiscale Humidity Visualization by Environmentally Sensitive Fluorescent Molecular Rotors. *Adv. Mater.* 2017,

29, No. 1703900.

- (10) Peng, Y.; Zhao, Y.; Chen, M. Q.; Xia, F. Research Advances in Microfiber Humidity Sensors. *Small* 2018, 14, No. 1800524.
- (11) Wang, S.; Oh, J. Y.; Xu, J.; Tran, H.; Bao, Z. Skin-Inspired Electronics: An Emerging Paradigm. *Acc. Chem. Res.* 2018, 51, 1033–1045.
- (12) Lee, Y.; Park, J.; Choe, A.; Cho, S.; Kim, J.; Ko, H. Mimicking Human and Biological Skins for Multifunctional Skin Electronics. *Adv. Funct. Mater.* 2020, 30, No. 1904523.
- (13) Kang, S. K.; Koo, J.; Lee, Y. K.; Rogers, J. A. Advanced Materials and Devices for Bioresorbable Electronics. *Acc. Chem. Res.* 2018, 51, 988–998.
- (14) Jung, Y. H.; Hong, S. K.; Wang, H. S.; Han, J. H.; Pham, T. X.; Park, H.; Kim, J.; Kang, S.; Yoo, C. D.; Lee, K. J. Flexible Piezoelectric Acoustic Sensors and Machine Learning for Speech Processing. *Adv. Mater.* 2020, 32, No. 1904020.
- (15) Wang, X.; Liu, Z.; Zhang, T. Flexible Sensing Electronics for Wearable/Attachable Health Monitoring. *Small* 2017, 13, No. 1602790.
- (16) Gao, Y.; Yu, L.; Yeo, J. C.; Lim, C. T. Flexible Hybrid Sensors for Health Monitoring: Materials and Mechanisms to Render Wearability. *Adv. Mater.* 2020, 32, No. 1902133.
- (17) Trung, T. Q.; Lee, N. E. Flexible and Stretchable Physical Sensor Integrated Platforms for Wearable Human-Activity Monitoring and Personal Healthcare. *Adv. Mater.* 2016, 28, 4338–4372.
- (18) Wang, M.; Luo, Y.; Wang, T.; Wan, C.; Pan, L.; Pan, S.; He, K.; Neo, A.; Chen, X. Artificial Skin Perception. *Adv. Mater.* 2021, No. 2003014.
- (19) Jin, X.; Liu, C.; Xu, T.; Su, L.; Zhang, X. Artificial Intelligence Biosensors: Challenges and Prospects. *Biosens. Bioelectron.* 2020, 165, No. 112412.
- (20) Zhu, C.; Chalmers, E.; Chen, L.; Wang, Y.; Xu, B. B.; Li, Y.; Liu, X. A Nature-Inspired, Flexible Substrate Strategy for Future Wearable Electronics. *Small* 2019, 15, No. 1902440.
- (21) Zhu, C.; Li, R.; Chen, X.; Chalmers, E.; Liu, X.; Wang, Y.; Xu, B. B.; Liu, X. Ultraelastic Yarns from Curcumin-Assisted ELD toward Wearable Human-Machine Interface Textiles. *Adv. Sci.* 2020, 7, No. 2002009.
- (22) Lin, S.; Yuk, H.; Zhang, T.; Parada, G. A.; Koo, H.; Yu, C.; Zhao, X. Stretchable Hydrogel Electronics and Devices. *Adv. Mater.* 2016, 28, 4497–4505.
- (23) Gu, X.; Shaw, L.; Gu, K.; Toney, M. F.; Bao, Z. The Meniscus-Guided Deposition of Semiconducting Polymers. *Nat. Commun.* 2018, 9, No. 534.
- (24) Zhang, J.; Wan, L.; Gao, Y.; Fang, X.; Lu, T.; Pan, L.; Xuan, F. Highly Stretchable and Self-healable MXene/polyvinyl Alcohol Hydrogel Electrode for Wearable Capacitive Electronic Skin. *Adv. Electron. Mater.* 2019, 5, No. 1900285.
- (25) Zhang, Q.; Niu, S.; Wang, L.; Lopez, J.; Chen, S.; Cai, Y.; Du, R.; Liu, Y.; Lai, J.-C.; Liu, L.; Li, C.-H.; Yan, X.; Liu, C.; Tok, J. B.-H.; Jia, X.; Bao, Z. An Elastic Autonomous Self-Healing Capacitive Sensor Based on a Dynamic Dual Crosslinked Chemical System. *Adv. Mater.*

2018, 30, No. 1801435.

- (26) Liao, M.; Wan, P.; Wen, J.; Gong, M.; Wu, X.; Wang, Y.; Shi, R.; Zhang, L. Wearable, Healable, and Adhesive Epidermal Sensors Assembled from Mussel-Inspired Conductive Hybrid Hydrogel Framework. *Adv. Funct. Mater.* 2017, 27, No. 1703852.
- (27) Miao, P.; Wang, J.; Zhang, C.; Sun, M.; Cheng, S.; Liu, H. Graphene Nanostructure-Based Tactile Sensors for Electronic Skin Applications. *Nano-Micro Lett.* 2019, 11, No. 71.
- (28) Jing, X.; Mi, H. Y.; Peng, X. F.; Turng, L.-S. Biocompatible, Self-healing, Highly Stretchable Polyacrylic Acid/Reduced Graphene Oxide Nanocomposite Hydrogel Sensors via Mussel-Inspired Chemistry. *Carbon* 2018, 136, 63–72.
- (29) Cai, G.; Wang, J.; Qian, K.; Chen, J.; Li, S.; Lee, P. S. Extremely Stretchable Strain Sensors Based on Conductive Self-Healing Dynamic Cross-Links Hydrogels for Human-Motion Detection. *Adv. Sci.* 2017, 4, No. 1600190.
- (30) Nela, L.; Tang, J.; Cao, Q.; Tulevski, G.; Han, S. J. Large-Area High-Performance Flexible Pressure Sensor with Carbon Nanotube Active Matrix for Electronic Skin. *Nano Lett.* 2018, 18, 2054–2059.
- (31) Wang, Z.; Chen, J.; Cong, Y.; Zhang, H.; Xu, T.; Nie, L.; Fu, J. Ultrastretchable Strain Sensors and Arrays with High Sensitivity and Linearity Based on Super Tough Conductive Hydrogels. *Chem. Mater.* 2018, 30, 8062–8069.
- (32) Lee, Y. Y.; Kang, H. Y.; Gwon, S. H.; Choi, G. M.; Lim, S. M.; Sun, J. Y.; Joo, Y. C. A Strain-Insensitive Stretchable Electronic Conductor: PEDOT: PSS/Acrylamide Organogels. *Adv. Mater.* 2016, 28, 1636–1643.
- (33) Gong, M.; Zhang, L.; Wan, P. Polymer Nanocomposite Meshes for Flexible Electronic Devices. *Prog. Polym. Sci.* 2020, No. 101279.
- (34) Fang, X.; Tan, J.; Gao, Y.; Lu, Y.; Xuan, F. High-Performance Wearable Strain Sensors Based on Fragmented Carbonized Melamine Sponges for Human Motion Detection. *Nanoscale* 2017, 9, 17948–17956.
- (35) Koo, J. H.; Kim, D. C.; Shim, H. J.; Kim, T.-H.; Kim, D.-H. Flexible and Stretchable Smart Display: Materials, Fabrication, Device Design, and System Integration. *Adv. Funct. Mater.* 2018, 28, No. 1801834.
- (36) Gao, Y.; Jia, F.; Gao, G. Transparent and Conductive Amino Acid-Tackified Hydrogels as Wearable Strain Sensors. *Chem. Eng. J.* 2019, 375, No. 121915.
- (37) Liu, H.; Li, M.; Ouyang, C.; Lu, T. J.; Li, F.; Xu, F. Biofriendly, Stretchable, and Reusable Hydrogel Electronics as Wearable Force Sensors. *Small* 2018, 14, No. 1801711.
- (38) Kim, K.; Park, Y. G.; Hyun, B. G.; Choi, M.; Park, J. U. Recent Advances in Transparent Electronics with Stretchable Forms. *Adv. Mater.* 2019, 31, No. 1804690.
- (39) Lee, H. R.; Kim, C. C.; Sun, J. Y. Stretchable Ionics - A Promising Candidate for Upcoming Wearable Devices. *Adv. Mater.* 2018, 30, No. 1704403.
- (40) Yin, X.-Y.; Zhang, Y.; Cai, X.; Guo, Q.; Yang, J.; Wang, Z. L. 3D Printing of Ionic Conductors for High-Sensitivity Wearable Sensors. *Mater. Horiz.* 2019, 6, 767–780.

- (41) Yuk, H.; Lu, B.; Zhao, X. Hydrogel Bioelectronics. *Chem. Soc. Rev.* 2019, 48, 1642–1667.
- (42) Sun, J. Y.; Keplinger, C.; Whitesides, G. M.; Suo, Z. Ionic Skin. *Adv. Mater.* 2014, 26, 7608–7614.
- (43) Zhou, Y.; Wan, C.; Yang, Y.; Yang, H.; Wang, S.; Dai, Z.; Ji, K.; Jiang, H.; Chen, X.; Long, Y. Highly Stretchable, Elastic, and Ionic Conductive Hydrogel for Artificial Soft Electronics. *Adv. Funct. Mater.* 2019, 29, No. 1806220.
- (44) Ge, G.; Zhang, Y.; Shao, J.; Wang, W.; Si, W.; Huang, W.; Dong, X. Stretchable, Transparent, and Self-Patterned Hydrogel-Based Pressure Sensor for Human Motions Detection. *Adv. Funct. Mater.* 2018, 28, No. 1802576.
- (45) Li, D.; Lai, W. Y.; Zhang, Y. Z.; Huang, W. Printable Transparent Conductive Films for Flexible Electronics. *Adv. Mater.* 2018, 30, No. 1704738.
- (46) Tong, R.; Chen, G.; Pan, D.; Qi, H.; Li, R.; Tian, J.; Lu, F.; He, M. Highly Stretchable and Compressible Cellulose Ionic Hydrogels for Flexible Strain Sensors. *Biomacromolecules* 2019, 20, 2096–2104.
- (47) Wang, L.; Gao, G.; Zhou, Y.; Xu, T.; Chen, J.; Wang, R.; Zhang, R.; Fu, J. Tough, Adhesive, Self-Healable, and Transparent Ionically Conductive Zwitterionic Nanocomposite Hydrogels as Skin Strain Sensors. *ACS Appl. Mater. Interfaces* 2019, 11, 3506–3515.
- (48) Blackman, L. D.; Gunatillake, P. A.; Cass, P.; Locock, K. E. S. An Introduction to Zwitterionic Polymer Behavior and Applications in Solution and at Surfaces. *Chem. Soc. Rev.* 2019, 48, 757–770.
- (49) Roy, C. K.; Guo, H. L.; Sun, T. L.; Ihsan, A. B.; Kurokawa, T.; Takahata, M.; Nonoyama, T.; Nakajima, T.; Gong, J. P. Self-Adjustable Adhesion of Polyampholyte Hydrogels. *Adv. Mater.* 2015, 27, 7344–7348.
- (50) Miao, T.; Wang, J.; Zeng, Y.; Liu, G.; Chen, X. Polysaccharide-Based Controlled Release Systems for Therapeutics Delivery and Tissue Engineering: From Bench to Bedside. *Adv. Sci.* 2018, 5, No. 1700513.
- (51) Vázquez-González, M.; Willner, I. Stimuli-Responsive Biomolecule-Based Hydrogels and Their Applications. *Angew. Chem., Int. Ed.* 2020, 59, 15342.
- (52) Du, G.; Wu, F.; Cong, Y.; Nie, L.; Liu, S.; Gao, G.; Fu, J. Versatile Controlled Ion Release for Synthesis of Recoverable Hybrid Hydrogels with High Stretchability and Notch-Insensitivity. *Chem. Commun.* 2015, 51, 15534–15537.
- (53) Ilčíková, M.; Tkáč, J.; Kasák, P. Switchable Materials Containing Polyzwitterion Moieties. *Polymers* 2015, 7, 2344–2370.
- (54) Wang, Z.; Li, J.; Jiang, L.; Xiao, S.; Liu, Y.; Luo, J. Zwitterionic Hydrogel Incorporated Graphene Oxide Nanosheets with Improved Strength and Lubricity. *Langmuir* 2019, 35, 11452–11462.
- (55) Mo, F.; Chen, Z.; Liang, G.; Wang, D.; Zhao, Y.; Li, H.; Dong, B.; Zhi, C. Zwitterionic Sulfobetaine Hydrogel Electrolyte Building Separated Positive/Negative Ion Migration Channels for Aqueous ZnMnO₂ Batteries with Superior Rate Capabilities. *Adv. Energy Mater.* 2020, 10, No. 2000035.
- (56) Hu, X.; Xia, X. X.; Huang, S. C.; Qian, Z. G. Development of Adhesive and Conductive Resilin-Based Hydrogels for Wearable

- Sensors. *Biomacromolecules* 2019, 20, 3283–3293.
- (57) Gao, Z.; Li, Y.; Shang, X.; Hu, W.; Gao, G.; Duan, L. BioInspired Adhesive and Self-Healing Hydrogels as Flexible Strain Sensors for Monitoring Human Activities. *Mater. Sci. Eng., C* 2020, 106, No. 110168.
- (58) Zhou, H.; Li, S.; Liu, H.; Zheng, B.; Jin, X.; Ma, A.; Chen, W. High-Performance Flexible Sensors of Self-Healing, Reversibly Adhesive, and Stretchable Hydrogels for Monitoring Large and Subtle Strains. *Macromol. Mater. Eng.* 2019, 305, No. 1900621.
- (59) Yang, B.; Yuan, W. Highly Stretchable, Adhesive, and Mechanical Zwitterionic Nanocomposite Hydrogel Biomimetic Skin. *ACS Appl. Mater. Interfaces* 2019, 11, 40620–40628.
- (60) He, X.; Liu, L.; Han, H.; Shi, W.; Yang, W.; Lu, X. Bioinspired and Microgel-Tackified Adhesive Hydrogel with Rapid Self-Healing and High Stretchability. *Macromolecules* 2018, 52, 72–80.
- (61) Han, L.; Lu, X.; Wang, M.; Gan, D.; Deng, W.; Wang, K.; Fang, L.; Liu, K.; Chan, C. W.; Tang, Y.; Weng, L. T.; Yuan, H. A Mussel-Inspired Conductive, Self-Adhesive, and Self-Healable Tough Hydrogel as Cell Stimulators and Implantable Bioelectronics. *Small* 2017, 13, No. 1601916.
- (62) Di, X.; Kang, Y.; Li, F.; Yao, R.; Chen, Q.; Hang, C.; Xu, Y.; Wang, Y.; Sun, P.; Wu, G. Poly(N-isopropylacrylamide)/Polydopamine/Clay Nanocomposite Hydrogels with Stretchability, Conductivity, and Dual Light- and Thermo- Responsive Bending and Adhesive Properties. *Colloids Surf., B* 2019, 177, 149–159.
- (63) Jing, X.; Mi, H. Y.; Lin, Y. J.; Enriquez, E.; Peng, X. F.; Turng, L. S. Highly Stretchable and Biocompatible Strain Sensors Based on Mussel-Inspired Super-Adhesive Self-Healing Hydrogels for Human Motion Monitoring. *ACS Appl. Mater. Interfaces* 2018, 10, 20897–20909.
- (64) Zhang, Z.; Gao, Z.; Wang, Y.; Guo, L.; Yin, C.; Zhang, X.; Hao, J.; Zhang, G.; Chen, L. Eco-Friendly, Self-Healing Hydrogels for Adhesive and Elastic Strain Sensors, Circuit Repairing, and Flexible Electronic Devices. *Macromolecules* 2019, 52, 2531–2541.
- (65) Shao, C.; Wang, M.; Meng, L.; Chang, H.; Wang, B.; Xu, F.; Yang, J.; Wan, P. Mussel-Inspired Cellulose Nanocomposite Tough Hydrogels with Synergistic Self-Healing, Adhesive, and Strain Sensitive Properties. *Chem. Mater.* 2018, 30, 3110–3121.
- (66) Deng, Z.; Hu, T.; Lei, Q.; He, J.; Ma, P. X.; Guo, B. Stimuli Responsive Conductive Nanocomposite Hydrogels with High Stretchability, Self-Healing, Adhesiveness, and 3D Printability for Human Motion Sensing. *ACS Appl. Mater. Interfaces* 2019, 11, 6796–6808.
- (67) You, Z.; Dong, Y.; Li, X.; Yang, P.; Luo, M.; Zhu, Z.; Wu, L.; Zhou, X.; Chen, M. One-pot Synthesis of Multi-Functional Cellulose Based Ionic Conductive Organohydrogel with Low-Temperature Strain Sensitivity. *Carbohydr. Polym.* 2021, 251, No. 117019.
- (68) Zhang, P.; Zhao, C.; Zhao, T.; Liu, M.; Jiang, L. Recent Advances in Bioinspired Gel Surfaces with Superwettability and Special Adhesion. *Adv. Sci.* 2019, 6, No. 1900996.
- (69) Pinnaratip, R.; Bhuiyan, M. S. A.; Meyers, K.; Rajachar, R. M.; Lee, B. P. Multifunctional Biomedical Adhesives. *Adv. Healthcare Mater.* 2019, 8, No. 1801568.
- (70) Hou, Y.; Deng, X.; Xie, C. Biomaterial Surface Modification for

Underwater Adhesion. *Smart Mater. Med.* 2020, 1, 77–91.

(71) Ichikawa, T. Zwitterions as Building Blocks for Functional Liquid Crystals and Block Copolymers. *Polym. J.* 2017, 49, 413–421.

(72) Shi, X.; Wu, P. A Smart Patch with On-Demand Detachable Adhesion for Bioelectronics. *Small* 2021, 17, No. 2101220.

(73) Pan, X.; Wang, Q.; Guo, R.; Cao, S.; Wu, H.; Ouyang, X.; Huang, F.; Gao, H.; Huang, L.; Zhang, F.; Chen, L.; Ni, Y.; Liu, K. An Adaptive Ionic Skin with Multiple Stimulus Responses and Moistelectric Generation Ability. *J. Mater. Chem. A* 2020, 8, 17498–17506.

(74) Harada, S.; Honda, W.; Arie, T.; Akita, S.; Takei, K. Fully printed, highly sensitive multifunctional artificial electronic whisker arrays integrated with strain and temperature sensors. *ACS Nano* 2014, 8, 3921–3927.

(75) Trung, T. Q.; Ramasundaram, S.; Hwang, B. U.; Lee, N. E. An All-Elastomeric Transparent and Stretchable Temperature Sensor for Body-Attachable Wearable Electronics. *Adv. Mater.* 2016, 28, 502–509.

(76) Bang, J.; Lee, W. S.; Park, B.; Joh, H.; Woo, H. K.; Jeon, S.; Ahn, J.; Jeong, C.; Kim, T.-i.; Oh, S. J. Highly Sensitive Temperature Sensor: Ligand-Treated Ag Nanocrystal Thin Films on PDMS with Thermal Expansion Strategy. *Adv. Funct. Mater.* 2019, 29, No. 1903047.

(77) Chortos, A.; Liu, J.; Bao, Z. Pursuing Prosthetic Electronic Skin. *Nat. Mater.* 2016, 15, 937–950.

(78) Lei, Z.; Wu, P. A Supramolecular Biomimetic Skin Combining A Wide Spectrum of Mechanical Properties and Multiple Sensory Capabilities. *Nat. Commun.* 2018, 9, No. 1134.

(79) Lei, Z.; Wu, P. Zwitterionic Skins with a Wide Scope of Customizable Functionalities. *ACS Nano* 2018, 12, 12860–12868.

(80) Song, J.; Chen, S.; Sun, L.; Guo, Y.; Zhang, L.; Wang, S.; Xuan, H.; Guan, Q.; You, Z. Mechanically and Electronically Robust Transparent Organohydrogel Fibers. *Adv. Mater.* 2020, 32, No. 1906994.

(81) Sun, L.; Chen, S.; Guo, Y.; Song, J.; Zhang, L.; Xiao, L.; Guan, Q.; You, Z. Ionogel-based, Highly Stretchable, Transparent, Durable Triboelectric Nanogenerators for Energy Harvesting and Motion Sensing over a Wide Temperature Range. *Nano Energy* 2019, 63, No. 103847.

(82) Sun, L.; Huang, H.; Ding, Q.; Guo, Y.; Sun, W.; Wu, Z.; Qin, M.; Guan, Q.; You, Z. Highly Transparent, Stretchable, and Self-Healable Ionogel for Multifunctional Sensors, Triboelectric Nanogenerator, and Wearable Fibrous Electronics. *Adv. Fiber Mater.* 2021, DOI: 10.1007/s42765-021-00086-8.

(83) Chen, D.; Pei, Q. Electronic Muscles and Skins: A Review of Soft Sensors and Actuators. *Chem. Rev.* 2017, 117, 11239–11268.

(84) Shiffman, S.; Stone, A. A.; Hufford, M. R. Ecological Momentary Assessment. *Annu. Rev. Clin. Psychol.* 2008, 4, 1–32.

(85) Sarchiapone, M.; Gramaglia, C.; Iosue, M.; Carli, V.; Mandelli, L.; Serretti, A.; Marangon, D.; Zeppegno, P. The relationship between addiction to smartphone usage and depression among adults: a cross sectional study. *BMC Psychiatry* 2018, 18, No. 148.

(86) Kireev, D.; Okogbue, E.; Jayanth, R. T.; Ko, T.-J.; Jung, Y.; et al. Multipurpose and Reusable Ultrathin Electronic Tattoos Based on

PtSe₂ and PtTe₂. ACS Nano 2021, 15, 2800–2811.

(87) Luo, Y.; Wang, M.; Wan, C.; Cai, P.; Loh, X. J.; Chen, X. Devising Materials Manufacturing Toward Lab-to-Fab Translation of Flexible Electronics. Adv. Mater. 2020, 32, No. 2001903.

(88) Chen, Q.; Zhu, L.; Zhao, C.; Wang, Q.; Zheng, J. A Robust, One-Pot Synthesis of Highly Mechanical and Recoverable Double Network Hydrogels Using Thermoreversible Sol-Gel Polysaccharide. Adv. Mater. 2013, 25, 4171–4176.